

Primordial Nucleosynthesis

By GARY STEIGMAN

Department of Physics, The Ohio State University, Columbus, OH 43210, USA

The primordial abundances of deuterium, helium-3, helium-4, and lithium-7 probe the baryon density of the Universe only a few minutes after the Big Bang. Of these relics from the early Universe, deuterium is the baryometer of choice. After reviewing the current observational status of the relic abundances (a moving target!), the baryon density determined by big bang nucleosynthesis (BBN) is derived. The temperature fluctuation spectrum of the cosmic background radiation (CBR), established several hundred thousand years later, probes the baryon density at a completely different epoch in the evolution of the Universe. The excellent agreement between the BBN- and CBR-determined baryon densities provides impressive confirmation of the standard model of cosmology, permitting the study of extensions of the standard model. In combination with the BBN- and/or CBR-determined baryon density, the relic abundance of ^4He provides an excellent chronometer, constraining those extensions of the standard model which lead to a nonstandard early-Universe expansion rate.

1. Introduction

As the hot, dense, early Universe rushed to expand and cool, it briefly passed through the epoch of big bang nucleosynthesis (BBN), leaving behind as relics the first complex nuclei: deuterium, helium-3, helium-4, and lithium-7. The abundances of these relic nuclides were determined by the competition between the relative densities of nucleons (baryons) and photons and, by the universal expansion rate. In particular, while deuterium is an excellent baryometer, ^4He provides an accurate chronometer. Nearly 400 thousand years later, when the cosmic background radiation (CBR) had cooled sufficiently to allow neutral atoms to form, releasing the CBR from the embrace of the ionized plasma of protons and electrons, the spectrum of temperature fluctuations imprinted on the CBR encoded the baryon and radiation densities, along with the universal expansion rate at that epoch. As a result, the relic abundances of the light nuclides and the CBR temperature fluctuation spectrum provide invaluable windows on the early evolution of the Universe along with sensitive probes of its particle content.

The fruitful interplay between theory and data has been key to the enormous progress in cosmology in recent times. As new, more precise data became available, models have had to be refined or rejected. It is anticipated this this process will – indeed, should – continue. Therefore, this review of the baryon content of the Universe as revealed by BBN and the CBR is but a signpost on the road to a more complete understanding of the history and evolution of the Universe. By highlighting the current successes of the present “standard” model along with some of the challenges to it, I hope to identify those areas of theoretical and observational work which will contribute to continuing progress in our endeavor to understand the Universe, its past, present, and future.

2. A BBN Primer

Discussion of BBN can begin when the Universe is already a few tenths of a second old and the temperature is a few MeV. At such early epochs the Universe is too hot and dense to permit the presence of complex nuclei in any significant abundances and the baryons (nucleons) are either neutrons or protons whose relative abundances are determined by

the weak interactions

$$p + e^- \longleftrightarrow n + \nu_e, \quad n + e^+ \longleftrightarrow p + \bar{\nu}_e, \quad n \longleftrightarrow p + e^- + \bar{\nu}_e. \quad (2.1)$$

The higher neutron mass favors protons relative to neutrons, ensuring proton dominance. When the weak interaction rates (Eq. 2.1) are fast compared to the universal expansion rate (and in the absence of a significant chemical potential for the electron neutrinos), $n/p \approx \exp(-\Delta m/T)$, where Δm is the neutron-proton mass difference and T is the temperature ($T_\gamma = T_e = T_\nu = T_N$ prior to e^\pm annihilation). If there were an *asymmetry* between the number densities of ν_e and $\bar{\nu}_e$ (“neutrino degeneracy”), described by a chemical potential μ_e (or, equivalently, by the dimensionless degeneracy parameter $\xi_e \equiv \mu_e/T$) then, early on, $n/p \approx \exp(-\Delta m/T - \xi_e)$. For a *significant* positive chemical potential ($\xi_e \gtrsim 0.01$; more ν_e than $\bar{\nu}_e$) there are fewer neutrons than for the “standard” case (SBBN) which, as described below, leads to the formation of less ^4He .

The first step in building complex nuclei is the formation of deuterons via $n+p \longleftrightarrow \text{D}+\gamma$. Sufficiently early on, when the Universe is very hot ($T \gtrsim 80$ keV), the newly-formed deuterons find themselves bathed in a background of gamma rays (the photons whose relics have cooled today to form the CBR at a temperature of 2.7 K) and are quickly photo-dissociated, removing the platform necessary for building heavier nuclides. Only below ~ 80 keV has the Universe cooled sufficiently to permit BBN to begin, leading to the synthesis of the lightest nuclides D, ^3He , ^4He , and ^7Li . Once BBN begins, D, ^3H , and ^3He are rapidly burned (for the baryon densities of interest) to ^4He , the light nuclide with the largest binding energy. The absence of a stable mass-5 nuclide, in combination with Coulomb barriers, suppresses the BBN production of heavier nuclides; only ^7Li is synthesized in an astrophysically interesting abundance. All the while the Universe is expanding and cooling. When the temperature has dropped below ~ 30 keV, at a time comparable to the neutron lifetime, the thermal energies of the colliding nuclides is insufficient to overcome the Coulomb barriers, the remaining free neutrons decay, and BBN ends.

From this brief overview of BBN it is clear that the relic abundances of the nuclides produced during BBN depend on the competition between the nuclear and weak interaction rates (which depend on the baryon density) and the universal expansion rate (quantified by the Hubble parameter H), so that the relic abundances provide early-Universe baryometers and chronometers.

2.1. *Early-Universe Expansion Rate*

The Friedman equation relates the expansion rate (measured by the Hubble parameter H) to the energy density (ρ): $H^2 = \frac{8\pi G}{3}\rho$ where, during the early, “radiation-dominated” (RD) evolution the energy density is dominated by the relativistic particles present ($\rho = \rho_R$). For SBBN, prior to e^\pm annihilation, these are: photons, e^\pm pairs and, three flavors of left-handed (i.e., one helicity state) neutrinos (and their right-handed, antineutrinos).

$$\rho_R = \rho_\gamma + \rho_e + 3\rho_\nu = \frac{43}{8}\rho_\gamma, \quad (2.2)$$

where ρ_γ is the energy density in CBR photons. At this early epoch, when $T \lesssim$ few MeV, the neutrinos are beginning to decouple from the $\gamma - e^\pm$ plasma and the neutron to proton ratio, crucial for the production of primordial ^4He , is decreasing. The time-temperature relation follows from the Friedman equation and the temperature dependence of ρ_γ

$$\text{Pre-} e^\pm \text{ annihilation : } t T_\gamma^2 = 0.738 \text{ MeV}^2 \text{ s}. \quad (2.3)$$

To a very good (but not exact) approximation the neutrinos (ν_e, ν_μ, ν_τ) are decoupled when the e^\pm pairs annihilate as the Universe cools below $m_e c^2$. In this approximation the neutrinos don't share in the energy transferred from the annihilating e^\pm pairs to the CBR photons so that in the post- e^\pm annihilation universe the photons are hotter than the neutrinos by a factor $T_\gamma/T_\nu = (11/4)^{1/3}$, and the relativistic energy density is

$$\rho_R = \rho_\gamma + 3\rho_\nu = 1.68\rho_\gamma. \quad (2.4)$$

The post- e^\pm annihilation time-temperature relation is

$$\text{Post} - e^\pm \text{ annihilation : } t T_\gamma^2 = 1.32 \text{ MeV}^2 \text{ s}. \quad (2.5)$$

2.1.1. Additional Relativistic Energy Density

One of the most straightforward variations of the standard model of cosmology is to allow for an early (RD) nonstandard expansion rate $H' \equiv SH$, where $S \equiv H'/H = t/t'$ is the *expansion rate factor*. One possibility for $S \neq 1$ is from the modification of the RD energy density (see Eqs. 2.2 & 2.4) due to “extra” relativistic particles X : $\rho_R \rightarrow \rho_R + \rho_X$. If the extra energy density is normalized to that which would be contributed by one additional flavor of (decoupled) neutrinos (Steigman, Schramm & Gunn 1977), $\rho_X \equiv \Delta N_\nu \rho_\nu$ ($N_\nu \equiv 3 + \Delta N_\nu$), then

$$S_{pre} \equiv (H'/H)_{pre} = (1 + 0.163\Delta N_\nu)^{1/2}; \quad S_{post} \equiv (H'/H)_{post} = (1 + 0.135\Delta N_\nu)^{1/2}. \quad (2.6)$$

Notice that S and ΔN_ν are related *nonlinearly*. It must be emphasized that it is S and not ΔN_ν that is the fundamental parameter in the sense that *any* term in the Friedman equation which scales as radiation, decreasing with the fourth power of the scale factor, will change the standard-model expansion rate ($S \neq 1$). For example, higher-dimensional effects such as in the Randall-Sundrum model (Randall & Sundrum 1999a) may lead to either a speed-up in the expansion rate ($S > 1$; $\Delta N_\nu > 0$) or, to a slow-down ($S < 1$; $\Delta N_\nu < 0$); see, also, Randall & Sundrum (1999b), Binetruy *et al.* (2000), Cline *et al.* (2000).

2.2. The Baryon Density

In the expanding Universe, the number densities of all particles decrease with time, so that the magnitude of the baryon density (or that of any other particle) has no meaning without also specifying *when it is measured*. To quantify the universal abundance of baryons, it is best to compare n_B to the CBR photon density n_γ . The ratio, $\eta \equiv n_B/n_\gamma$ is very small, so that it is convenient to define a quantity of order unity,

$$\eta_{10} \equiv 10^{10}(n_B/n_\gamma) = 274 \Omega_B h^2 \equiv 274 \omega_B, \quad (2.7)$$

where Ω_B is the ratio (at present) of the baryon density to the critical density and h is the present value of the Hubble parameter in units of $100 \text{ km s}^{-1} \text{ Mpc}^{-1}$ ($\omega_B \equiv \Omega_B h^2$).

3. BBN Abundances

The relic abundances of D, ^3He , and ^7Li are *rate limited*, determined by the competition between the early Universe expansion rate and the nucleon density. Any of these three nuclides is, therefore, a potential baryometer; see Figure 1.

In contrast to the synthesis of the other light nuclides, once BBN begins ($T \lesssim 80 \text{ keV}$) the reactions building ^4He are so rapid that its relic abundance is not rate limited. The primordial abundance of ^4He is limited by the availability of neutrons. To a very good approximation, its relic abundance is set by the neutron abundance at the beginning

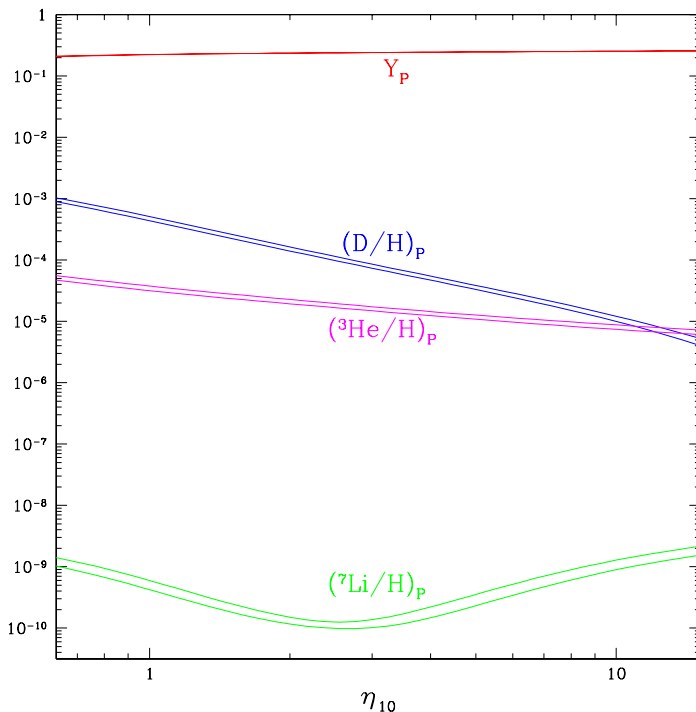


FIGURE 1. The SBBN-predicted abundances of D, ${}^3\text{He}$, and ${}^7\text{Li}$ by number with respect to hydrogen, and the ${}^4\text{He}$ mass fraction Y_{P} , as a function of the nucleon (baryon) abundance parameter η_{10} . The bands reflect the theoretical uncertainties ($\pm 1\sigma$) in the BBN predictions.

of BBN. As a result, the primordial mass fraction of ${}^4\text{He}$, Y_{P} , while being a relatively insensitive baryometer (see Figure 1), is an excellent, early-Universe chronometer.

The qualitative effects of a nonstandard expansion rate on the relic abundances of the light nuclides may be understood with reference to Figure 1. For the baryon abundance range of interest the relic abundances of D and ${}^3\text{He}$ are *decreasing* functions of η ; in this range, D and ${}^3\text{He}$ are being destroyed to build ${}^4\text{He}$. A faster than standard expansion ($S > 1$) provides less time for this destruction so that more D and ${}^3\text{He}$ will survive. The same behavior occurs for ${}^7\text{Li}$ at low values of η , where its abundance is a decreasing function of η . However, at higher values of η , the BBN-predicted ${}^7\text{Li}$ abundance *increases* with η , so that less time available results in less production and a *smaller* ${}^7\text{Li}$ relic abundance. Except for dramatic changes to the early-Universe expansion rate, these effects on the relic abundances of D, ${}^3\text{He}$, and ${}^7\text{Li}$ are subdominant to their variations with the baryon density. Not so for ${}^4\text{He}$, whose relic abundance is very weakly (logarithmically) dependent on the baryon density, but very strongly dependent on the early-Universe expansion rate. A faster expansion leaves more neutrons available to build ${}^4\text{He}$; to a good approximation $\Delta Y \approx 0.16(S - 1)$. It is clear then that if ${}^4\text{He}$ is paired with any of the other light nuclides, together they can constrain the baryon density (η or $\Omega_{\text{B}}h^2 \equiv \omega_{\text{B}}$) and the early-Universe expansion rate (S or ΔN_{ν}).

As noted above in §2, the neutron-proton ratio at BBN can also be modified from its standard value in the presence of a significant electron-neutrino asymmetry ($\xi_e \gtrsim 0.01$). As a result, Y_{P} is also sensitive to any neutrino asymmetry. More ν_e than $\bar{\nu}_e$ drives

the neutron-to-proton ratio down (see Eq. 2.1), leaving fewer neutrons available to build ${}^4\text{He}$; to a good approximation $\Delta Y \approx -0.23 \xi_e$ (Kneller & Steigman 2003). In contrast, the relic abundances of D, ${}^3\text{He}$, and ${}^7\text{Li}$ are very insensitive to $\xi_e \neq 0$, so that when paired with ${}^4\text{He}$, they can simultaneously constrain the baryon density and the electron-neutrino asymmetry. Notice that if *both* S and ξ_e are allowed to be free parameters, another observational constraint is needed to simultaneously constrain η , S , and ξ_e . While neither ${}^3\text{He}$ nor ${}^7\text{Li}$ can provide the needed constraint, the CBR temperature anisotropy spectrum, which is sensitive to η and S , but not to ξ_e , can (see Barger *et al.* 2003b). This review will concentrate on combining constraints from the CBR and SBBN ($S = 1$, $\xi_e = 0$) and also for $S \neq 1$ ($\xi_e = 0$). For the influence of and constraints on electron neutrino asymmetry, see Barger *et al.* (2003b) and further references therein.

4. Relic Abundances

BBN constraints on the universal density of baryons and on the early-Universe expansion rate require reasonably accurate determinations of the relic abundances of the light nuclides. As already noted, D, ${}^3\text{He}$, and ${}^7\text{Li}$ are all potential baryometers, while ${}^4\text{He}$ is an excellent chronometer. The combination of the availability of large telescopes and advances in detector technology has made it possible to obtain abundance estimates at various sites in the Galaxy and elsewhere in the Universe with unprecedented precision (statistically). However, the path to accurate primordial abundances is littered with systematic uncertainties which have the potential to contaminate otherwise exquisite data. It is, therefore, fortunate that the relic nuclides follow very different post-BBN evolutionary paths and are observed in diverse environments using a wide variety of astronomical techniques. Neutral deuterium is observed in absorption in the UV (or, in the optical when redshifted) against background, bright sources (O or B stars in the Galaxy, QSOs extragalactically). Singly-ionized helium-3 is observed in emission in Galactic H II regions via its spin-flip transition (the analog of the 21 cm line in neutral hydrogen). The helium-4 abundance is largely determined by observations of recombination lines of ionized (singly and doubly) ${}^4\text{He}$ compared to those of ionized hydrogen in Galactic and, especially, extragalactic H II regions. Observations of ${}^7\text{Li}$, at least those at low metallicity (nearly primordial) are restricted to absorption in the atmospheres of the oldest, most metal-poor stars in the halo of the Galaxy. The different evolutionary histories (described below) combined with the different observational strategies provide a measure of insurance that systematic errors in the determination of one of the light element abundances are unlikely to propagate into other abundance determinations.

4.1. Deuterium – The Baryometer Of Choice

The deuteron is the most weakly bound of the light nuclides. As a result, any deuterium cycled through stars is burned to ${}^3\text{He}$ and beyond. Thus, its post-BBN evolution is straightforward: deuterium observed anywhere, anytime, provides a *lower* bound to the primordial D abundance. For “young” systems, in the sense of little stellar evolution (e.g. sites at high redshift and/or with very low metallicity), the observed D abundance should reach a plateau at the primordial value. Although there are observations of deuterium in the solar system and the interstellar medium (ISM) of the Galaxy which provide interesting lower bounds to its primordial abundance, the observations of relic D in a few, high redshift, low metallicity, QSO absorption line systems (QSOALS) are of most value in estimating its primordial abundance.

While its simple post-BBN evolution is the greatest asset for relic D, the identical absorption spectra of D I and H I (except for the velocity/wavelength shift resulting from the

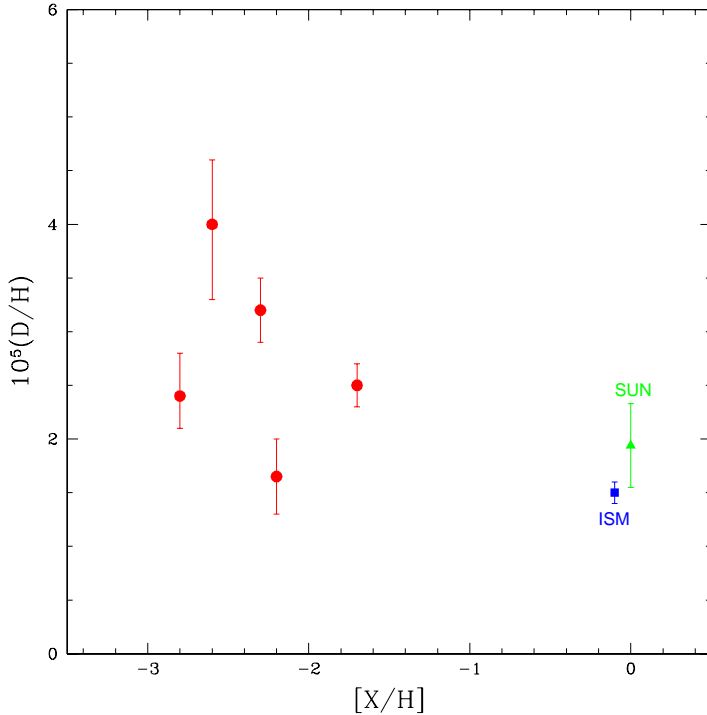


FIGURE 2. Deuterium abundances, by number with respect to hydrogen D/H , versus metallicity (relative to solar on a log scale) from observations (as of early 2003) of QSOALS (filled circles). “X” is usually silicon or oxygen. Shown for comparison are the D abundances inferred for the local ISM (filled square) and the solar system (presolar nebula: “Sun”; filled triangle).

heavier reduced mass of the deuterium atom) is a severe liability, limiting significantly the number of useful targets in the vast Lyman-alpha forest of the QSO absorption spectra (see Kirkman *et al.* (2003) for a discussion). It is essential in choosing a target QSOALS that its velocity structure be “simple” since a low column density $H I$ absorber, shifted by ~ 81 km/s with respect to the main $H I$ absorber (an “interloper”) would masquerade as $D I$ absorption. If this is not recognized, a too high D/H ratio would be inferred. Since there are many more low-column density absorbers than those with high $H I$ column densities, absorption systems with somewhat lower $H I$ column density (e.g. Lyman-limit systems: LLS) are more susceptible to this contamination than the higher $H I$ column density absorbers (e.g. damped $Ly\alpha$ absorbers: DLA). However, while the DLA have many advantages over the LLS, a precise determination of the $H I$ column density requires an accurate placement of the continuum, which could be compromised by interlopers. This might lead to an overestimate of the $H I$ column density and a concomitant underestimate of D/H (J. Linsky, private communication). As a result of these complications, the path to primordial D using QSOALS has not been straightforward, and some abundance claims have had to be withdrawn or revised. Presently there are only five QSOALS with reasonably firm deuterium detections Kirkman *et al.* (2003) (and references therein); these are shown in Figure 2 along with the corresponding solar system and ISM D abundances. It is clear from Figure 2, that there is significant dispersion among the derived D abundances at low metallicity which, so far, mask the anticipated

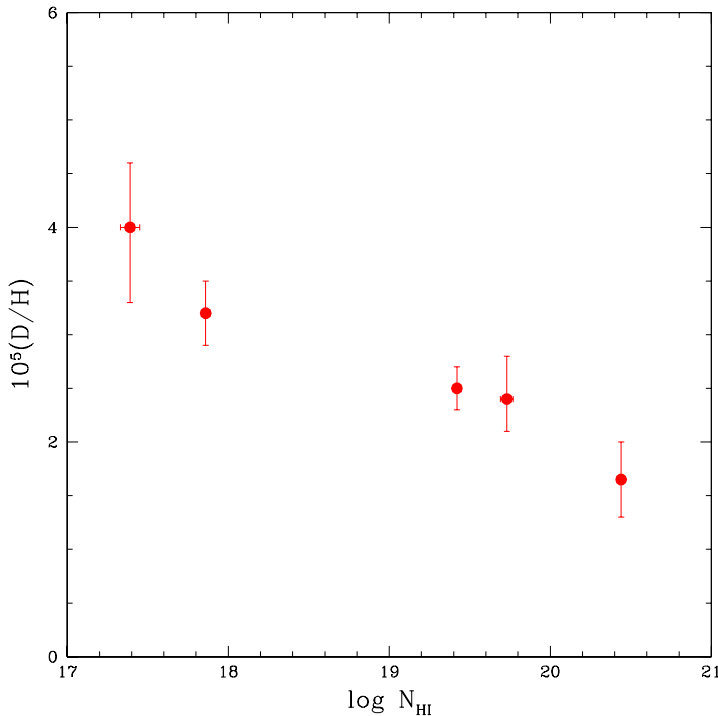


FIGURE 3. Deuterium abundances versus the H I column densities for the corresponding QSOALS shown in Figure 2.

deuterium plateau. This suggests that systematic errors of the sort described here may have contaminated some of the determinations of the D I and/or H I column densities.

To explore the possibility that such systematic effects, which would be correlated with the H I column density, may be responsible for at least some of the dispersion revealed in Figure 2, it is useful to plot the same QSOALS data versus the H I column density; this is shown in Figure 3. Indeed, there is the suggestion from this very limited data set that the low column density absorbers (LLS) have high D/H, while the high column density systems (DLA) have low abundances. However, on the basis of extant data it is impossible to decide which, if any, of these systems has been contaminated; there is no justification for excluding any of the present data. Indeed, perhaps the data is telling us that our ideas about post-BBN deuterium evolution need to be revised.

To proceed further using the current data I follow the lead of O’Meara *et al.* (2001) and Kirkman *et al.* (2003) and adopt for the primordial D abundance the weighted mean of the D abundances for the five lines of sight (Kirkman *et al.* 2003); the dispersion in the data is used to set the error in y_D : $y_D = 2.6 \pm 0.4$. It should be noted that using the same data Kirkman *et al.* (2003) derive a slightly higher mean D abundance: $y_D = 2.74$. The difference is traced to their first finding the mean of $\log(y_D)$ and then using it to compute the mean D abundance ($y_D \equiv 10^{(\log(y_D))}$).

The BBN-predicted relic abundance of deuterium depends sensitively on the baryon density, $y_D \propto \eta^{-1.6}$, so that a $\sim 10\%$ determination of y_D can be used to estimate the baryon density to $\sim 6\%$. For SBBN ($S = 1$ ($N_\nu = 3$), $\xi_e = 0$), the adopted primordial D abundance corresponds to $\eta_{10}(\text{SBBN}) = 6.10^{+0.67}_{-0.52}$ ($\Omega_B h^2 = 0.0223^{+0.0024}_{-0.0019}$),

in spectacular agreement with the Spergel *et al.* (2003) estimate of $\eta_{10} = 6.14 \pm 0.25$ ($\Omega_B h^2 = 0.0224 \pm 0.0009$) based on WMAP and other CBR data (ACBAR and CBI) combined with large scale structure (2dFGRS) and Lyman-alpha forest constraints. Indeed, if the Spergel *et al.* (2003) estimate is used for the BBN baryon density, the BBN-predicted deuterium abundance is $y_D = 2.57 \pm 0.27$ (where a generous allowance of $\sim 8\%$ has been made for the uncertainty in the BBN prediction at fixed η ; for the Burles, Nollett & Turner (2001) nuclear cross sections and uncertainties the result is $y_D = 2.60^{+0.20}_{-0.18}$).

4.2. Helium-3

Unlike D, the post-BBN evolution of ${}^3\text{He}$ and ${}^7\text{Li}$ are quite complex. ${}^3\text{He}$ is destroyed in the hotter interiors of all but the least massive (coolest) stars, but it is preserved in the cooler, outer layers of most stars. In addition, hydrogen burning in low mass stars results in the production of significant amounts of *new* ${}^3\text{He}$ (Iben 1967; Rood 1972; Dearborn, Steigman & Schramm 1986; Vassiliadis & Wood 1993; Dearborn, Steigman & Tosi 1996). To follow the post-BBN evolution of ${}^3\text{He}$, it is necessary to account for all these effects – quantitatively – in the material returned by stars to the interstellar medium (ISM). As indicated by the existing Galactic data (Geiss & Gloeckler 1998; Bania, Rood & Balser 2002), a very delicate balance exists between net production and net destruction of ${}^3\text{He}$ in the course of the evolution of the Galaxy. As a consequence, aside from noting an excellent qualitative agreement between the SBBN predicted and observed ${}^3\text{He}$ abundances, ${}^3\text{He}$ has – at present – little role to play as a quantitatively useful baryometer. In this spirit, it is noted that an uncertain estimate of the primordial abundance of ${}^3\text{He}$ may be inferred from the observation of an outer-Galaxy (less evolved) H II region (Bania *et al.* 2002): $y_3 \equiv 10^5({}^3\text{He}/\text{H}) = 1.1 \pm 0.2$.

4.3. Lithium-7

A similar scenario may be sketched for ${}^7\text{Li}$. As a weakly bound nuclide, it is easily destroyed when cycled through stars except if it can be kept in the cooler, outer layers. The high lithium abundances observed in the few “super-lithium-rich red giants” provide direct evidence that at least some stars can synthesize post-BBN lithium and bring it to the surface. But, an unsolved issue is how much of this newly-synthesized lithium is actually returned to the ISM rather than mixed back into the interior and destroyed.

With these caveats in mind, in Figure 4 lithium abundances are shown as a function of metallicity from a compilation by V. V. Smith (private communication). Since the quest for nearly primordial lithium is restricted to the oldest, most metal-poor stars in the Galaxy, stars that have had the most time to redistribute – and destroy or dilute – their surface lithium abundances, it is unclear whether the “plateau” at low metallicities is representative of the primordial abundance of lithium. Although it seems clear that the lithium abundance in the Galaxy has increased since BBN, a quantitatively reliable estimate of its primordial abundance eludes us at present. Given this state of affairs, the most fruitful approach is to learn about stellar structure and evolution by comparing the BBN-predicted lithium abundance to those abundances inferred from observations of the oldest stars, rather than to attempt to use the stellar observations to constrain the BBN-inferred baryon density. Concentrating on the low-metallicity, nearly primordial data, it seems that $[\text{Li}] \equiv 12 + \log(\text{Li}/\text{H}) \approx 2.2 \pm 0.1$. This estimate will be compared to the BBN-predicted lithium abundance using D as a baryometer and, to the BBN-predicted lithium abundance using the CBR-inferred baryon density. Any tension between these BBN-predicted abundances and that inferred from the Galactic data may provide hints of nonstandard stellar astrophysics.

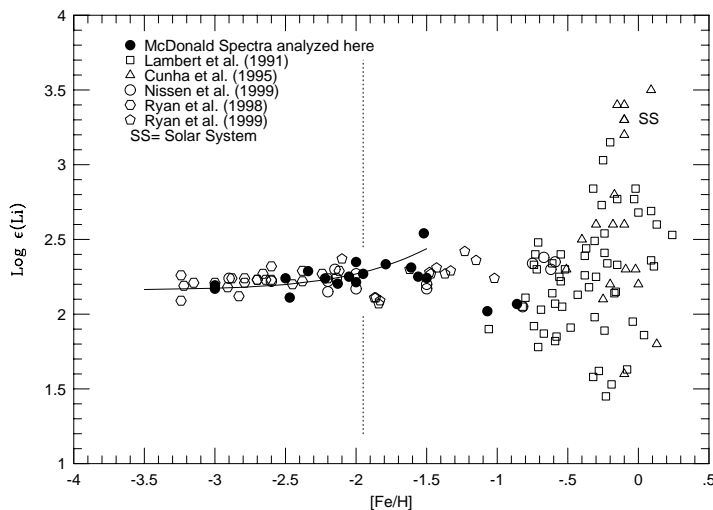


FIGURE 4. Lithium abundances, $\log \epsilon(\text{Li}) \equiv [\text{Li}] \equiv 12 + \log(\text{Li}/\text{H})$ versus metallicity (on a log scale relative to solar) from a compilation of stellar observations by V. V. Smith.

4.4. Helium-4 – The BBN Chronometer

The good news about ${}^4\text{He}$ is that, as the second most abundant nuclide, it may be observed throughout the Universe. The bad news is that its abundance has evolved since the end of BBN. In order to infer its primordial value it is therefore necessary to track the ${}^4\text{He}$ abundance determinations (mass fraction Y_{P}) as a function of metallicity or, to limit observations to very low metallicity objects. Although, as for D, there are observations of ${}^4\text{He}$ in the ISM and the solar system, the key data for determining its primordial abundance comes from observations of metal-poor, extragalactic H II regions. A compilation of current data (courtesy of K. A. Olive) is shown in Figure 5 where the ${}^4\text{He}$ mass fraction is plotted as a function of the oxygen abundance; note that the solar oxygen abundance, $\text{O}/\text{H} \approx 5 \times 10^{-4}$ (Allende-Prieto, Lambert & Asplund 2001) is off-scale in this figure. These are truly low metallicity H II regions.

It is clear from Figure 5 that the data exist to permit the derivation of a reasonably accurate estimate (statistically) of the primordial ${}^4\text{He}$ mass fraction Y_{P} , with or without any extrapolation to zero-metallicity. What is not easily seen in Figure 5 given the Y_{P} scale, is that Y_{P} derived from the data assembled from the literature by Olive & Steigman (1995) and Olive, Skillman & Steigman (1997) ($Y_{\text{P}} = 0.234 \pm 0.003$) is marginally inconsistent (at $\sim 2\sigma$) with the value derived by Izotov, Thuan & Lipovetsky (1997) and Izotov & Thuan (1998) from their nearly independent data set ($Y_{\text{P}} = 0.244 \pm 0.002$). In addition, there are a variety of systematic corrections which might modify *both* data sets (Steigman, Viegas & Gruenwald 1997; Viegas, Gruenwald & Steigman 2000; Olive & Skillman 2001; Sauer & Jedamzik 2002; Gruenwald, Steigman & Viegas 2002; Peimbert, Peimbert & Luridiana 2002)

Unless/until the differences in Y_{P} derived by different authors from somewhat different data sets is resolved and the known systematic errors are corrected for (the unknown ones will always hang over us like the sword of Damocles), the following compromise, adopted by Olive, Steigman & Walker (2000), may not be unreasonable. From

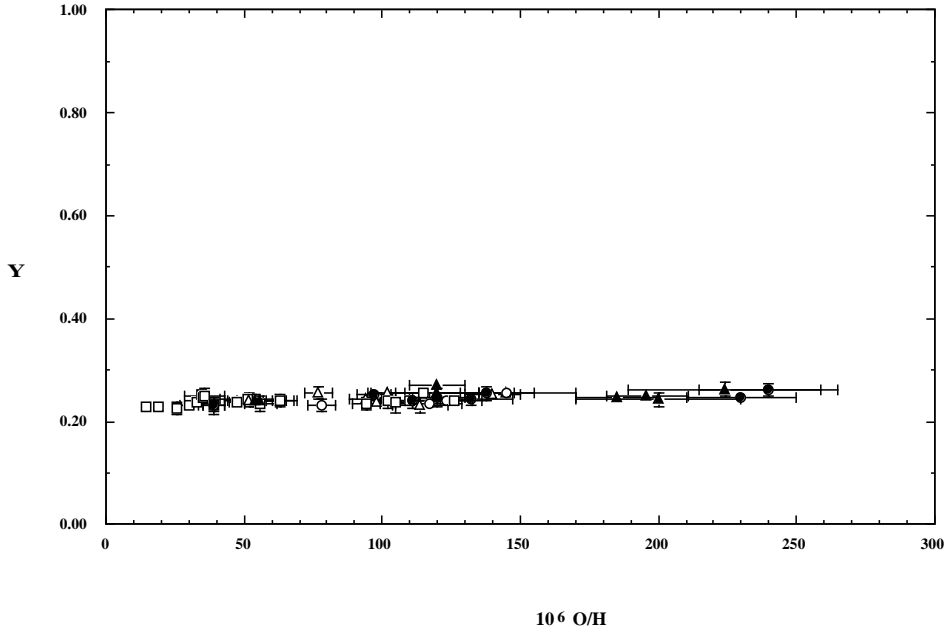


FIGURE 5. The ${}^4\text{He}$ mass fraction Y derived from observations of extragalactic H II regions of low metallicity versus the corresponding H II region oxygen abundances (from K. A. Olive).

Olive & Steigman (1995) and Olive, Skillman & Steigman (1997), the 2σ range for Y_{P} is $0.228 - 0.240$, while from the Izotov, Thuan & Lipovetsky (1997) and Izotov & Thuan (1998) data the 2σ range is $Y_{\text{P}} = 0.240 - 0.248$. Thus, although the current estimates are likely dominated by systematic errors, they span a $\sim 2\sigma$ range from $Y_{\text{P}} = 0.228$ to $Y_{\text{P}} = 0.248$. Therefore, as proposed by Olive, Steigman & Walker (2000), we adopt here a central value for $Y_{\text{P}} = 0.238$ and a $\sim 1\sigma$ uncertainty of 0.005 : $Y_{\text{P}} = 0.238 \pm 0.005$. Given the approximation (see §3) $\Delta Y \approx 0.16(S - 1)$, for $\sigma_{Y_{\text{P}}} \approx 0.005$ the uncertainty in S is ≈ 0.03 (corresponding to an uncertainty in ΔN_{ν} of ≈ 0.4).

5. The Baryon Density From SBBN

For SBBN, where $S = 1$ ($N_{\nu} = 3$) and $\xi_e = 0$, the primordial abundances of D , ${}^3\text{He}$, ${}^4\text{He}$, and ${}^7\text{Li}$ are predicted as a function of only one free parameter, the baryon density parameter (η or $\Omega_{\text{B}}h^2 \equiv \omega_{\text{B}}$). As described above (see §4.1), D is the baryometer of choice. From SBBN and the adopted relic abundance of deuterium, $y_{\text{D}} = 2.6 \pm 0.4$, $\eta_{10} = 6.1_{-0.5}^{+0.7}$ ($\Omega_{\text{B}}h^2 = 0.022 \pm 0.002$).

Having determined the baryon density to $\sim 10\%$ using D as the SBBN baryometer, it is incumbent upon us to compare the SBBN-predicted abundances of the other light nuclides with their relic abundances inferred from the observational data. For this baryon density, the predicted primordial abundance of ${}^3\text{He}$ is $y_3 = 1.04 \pm 0.10$, in excellent agreement with the primordial value of $y_3 = 1.1 \pm 0.2$ inferred from observations of an outer-Galaxy H II region (Bania *et al.* 2002). Within the context of SBBN, D and ${}^3\text{He}$ are completely consistent.

The first challenge to SBBN comes from ${}^4\text{He}$. For the SBBN-determined baryon density the predicted ${}^4\text{He}$ primordial mass fraction is $Y_{\text{P}} = 0.248 \pm 0.001$, to be compared with

our adopted value from extragalactic H II regions (Olive, Steigman & Walker 2000) of $Y_{\text{P}}^{\text{OSW}} = 0.238 \pm 0.005$. Agreement is only at the $\sim 2\sigma$ level. Given the unresolved systematic uncertainties in determining Y_{P} from the H II region data, it is not clear at present whether this is a challenge to SBBN or to our understanding of H II region recombination spectra. As will be seen below, this tension between SBBN D and ${}^4\text{He}$ can be relieved for nonstandard BBN if the assumption that $S = 1$ ($N_{\nu} = 3$) is relaxed.

The conflict with the inferred primordial abundance of lithium is even more challenging to SBBN. For $y_{\text{D}} = 2.6 \pm 0.4$, $[\text{Li}] = 2.65_{-0.12}^{+0.10}$. This is to be compared to the estimate (see Figure 4) of $[\text{Li}] = 2.2 \pm 0.1$ based on a sample of metal-poor, halo stars. The conflict is even greater with the Ryan *et al.* (2000) estimate of $[\text{Li}] = 2.09_{-0.13}^{+0.19}$ derived from an especially selected data set. Unlike the tension between SBBN and the D and ${}^4\text{He}$ abundances, the conflict between D and ${}^7\text{Li}$ cannot be resolved by a nonstandard expansion rate (nor, by an electron neutrino asymmetry). Most likely, the resolution of this conflict is astrophysical since the metal-poor halo stars from which the relic abundance of lithium is inferred have had the longest time to mix their surface material with that in their hotter interiors, diluting or destroying their prestellar quota of lithium (see, e.g. Pinsonneault *et al.* (2002) and references to related work therein).

At present SBBN in combination with the limited data set of QSOALS deuterium abundances yields a $\sim 10\%$ determination of the baryon density parameter. Consistency between the inferred primordial abundances of D and ${}^3\text{He}$ lends support to the internal consistency of SBBN, but the derived primordial abundances of ${}^4\text{He}$ and ${}^7\text{Li}$ pose some challenges. For ${}^4\text{He}$ the disagreement is only at the $\sim 2\sigma$ level and the errors in the observationally inferred value of Y_{P} are dominated by poorly quantified systematics. However, if the current discrepancy is real, it might be providing a hint at new physics beyond the standard model (e.g. nonstandard expansion rate and/or nonstandard neutrino physics). Before considering the effects on BBN of a nonstandard expansion rate ($S \neq 1$; $N_{\nu} \neq 3$), we will compare the SBBN estimate of the baryon density parameter with that from the CBR.

6. The Baryon Density From The CBR

Some 400 kyr after BBN has ended, when the Universe has expanded and cooled sufficiently so that the ionized plasma of protons, alphas, and electrons combines to form neutral hydrogen and helium, the CBR photons are set free to propagate throughout the Universe. Observations of the CBR today reveal the anisotropy spectrum of temperature fluctuations imprinted at that early epoch. The so-called acoustic peaks in the temperature anisotropy spectrum arise from the competition between the gravitational potential and the pressure gradients. An increase in the baryon density increases the inertia of the baryon – photon fluid shifting the locations and the relative heights of the acoustic peaks. In Figure 6 are shown three sets of temperature anisotropy spectra for cosmological models which differ only in the choice of the baryon density parameter ω_{B} . Also shown in Figure 6 are the WMAP data from Bennett *et al.* (2003). It is clear from Figure 6 that the CBR provides a very good baryometer – independent of that from SBBN and primordial deuterium. Based on the WMAP data alone, Barger *et al.* (2003a) find that the best fit value for the density parameter is $\eta_{10} = 6.3$ ($\omega_{\text{B}} = 0.023$) and that the 2σ range extends from $\eta_{10} = 5.6$ to 7.3 ($0.020 \leq \omega_{\text{B}} \leq 0.026$). This is in excellent (essentially perfect!) agreement (as it should be) with the CBR-only result of Spergel *et al.* (2003). More importantly, as may be seen clearly in Figure 7 (courtesy of D. Marfatia), this independent constraint on the baryon density parameter, sampled some 400 kyr after

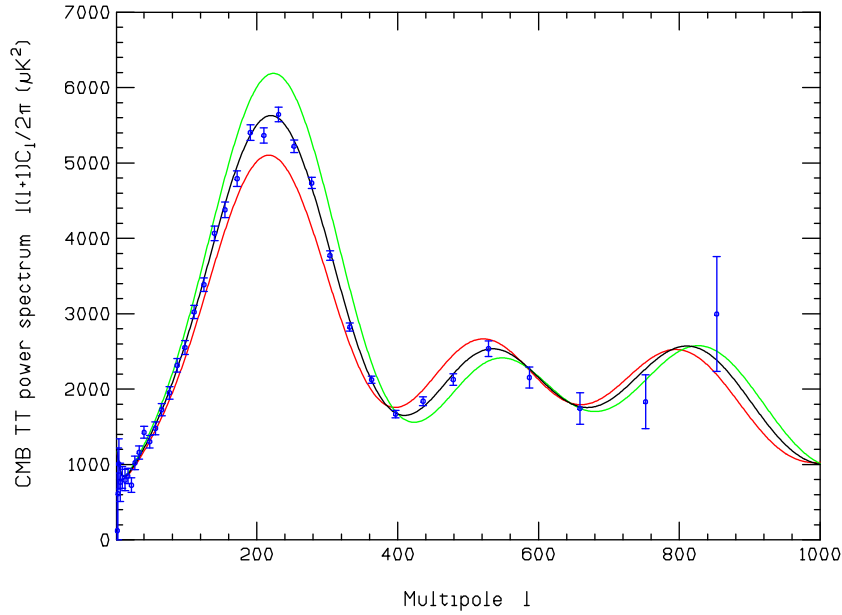


FIGURE 6. The CBR temperature fluctuation anisotropy spectra for three choices of the baryon density parameter $\omega_B = 0.018, 0.023, 0.028$, in order of increasing height of the first peak. Also shown are the WMAP data points.

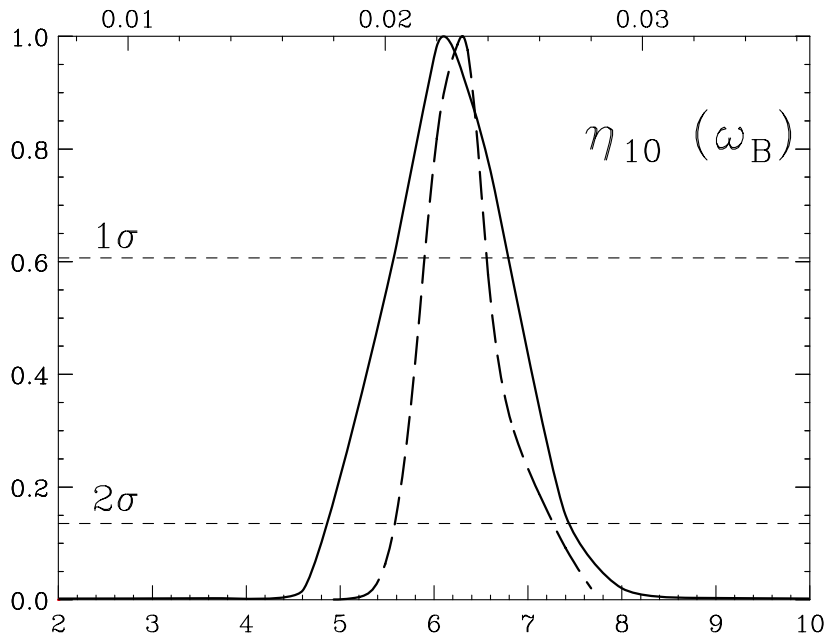


FIGURE 7. The normalized likelihood distributions for the baryon density parameter η_{10} derived from SBBN and the primordial abundance of deuterium (solid curve; see §4.1) and from the CBR using WMAP data alone (dashed curve). The bottom horizontal axis is the baryon-to-photon ratio parameter η_{10} ; the top axis is the baryon density parameter $\omega_B = \Omega_B h^2$.

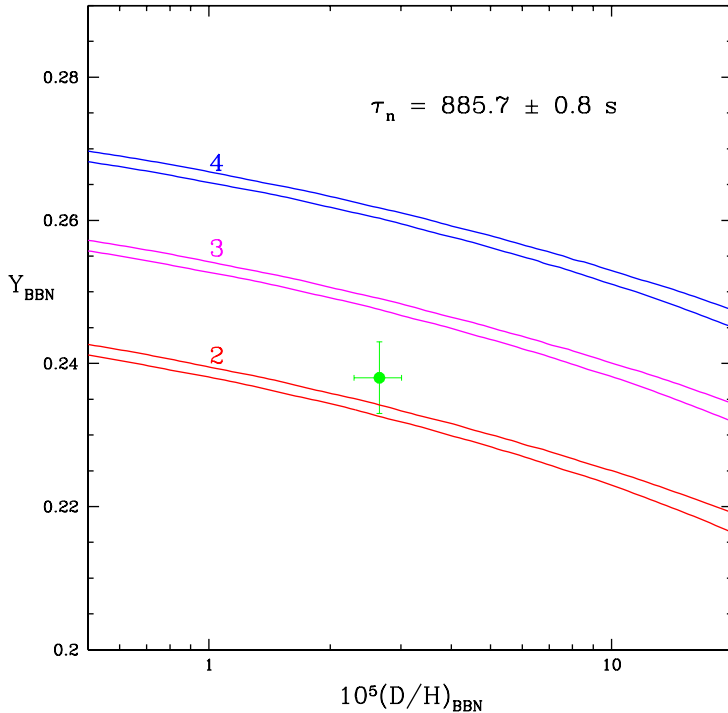


FIGURE 8. The BBN-predicted relation between the ${}^4\text{He}$ mass fraction Y_{P} and the deuterium abundance y_{D} for three, early-Universe expansion rates corresponding to $N_{\nu} = 2, 3, 4$. The filled circle with error bars is for the D and ${}^4\text{He}$ primordial abundances adopted here.

BBN, is in excellent agreement with that from SBBN (see §5), providing strong support for the standard model of cosmology.

The independent determination of the baryon density parameter by the CBR reinforces the tension between SBBN and the relic abundances of ${}^4\text{He}$ and ${}^7\text{Li}$ inferred from the observational data (see §5). In the context of SBBN, the slightly higher best value of η from the WMAP data (compared to that from D plus SBBN) *increases* the expected primordial abundances of ${}^4\text{He}$ and ${}^7\text{Li}$ (see Figure 1), widening the gaps between the SBBN predictions and the data. Keeping in mind the observational and theoretical difficulties in deriving the primordial abundances from the data, it is nonetheless worthwhile to explore a class of nonstandard alternatives to the standard model of cosmology in which the early Universe expansion rate is modified ($S \neq 1$, $N_{\nu} \neq 3$).

7. Nonstandard BBN: $S \neq 1$, $N_{\nu} \neq 3$

As outlined in §3, for fixed η as S increases the BBN-predicted abundances of D, ${}^3\text{He}$, and ${}^4\text{He}$ increase (less time to destroy D and ${}^3\text{He}$, more neutrons available for ${}^4\text{He}$), while that of ${}^7\text{Li}$ decreases (less time to produce ${}^7\text{Li}$). Since it is the ${}^4\text{He}$ mass fraction that is most sensitive to changes in the early Universe expansion rate and, since the SBBN-predicted value of Y_{P} is too large when compared to the data, $S < 1$ ($N_{\nu} < 3$) is required. For a *slower* than standard expansion rate the predicted abundances of D and ${}^3\text{He}$ *decrease* compared to their SBBN values (at fixed η) while that of ${}^7\text{Li}$ *increases*. Since the BBN-predicted abundance of D increases with decreasing baryon density, a decrease

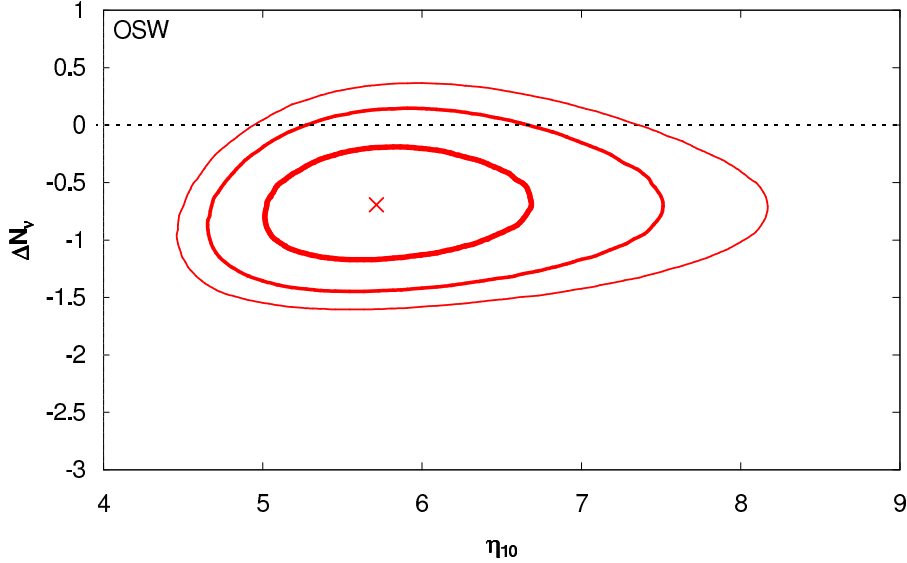


FIGURE 9. The 1σ , 2σ , and 3σ contours in the $\Delta N_\nu - \eta_{10}$ plane from BBN and the relic D and ${}^4\text{He}$ abundances. The best fit values of ΔN_ν and η_{10} are marked by the cross.

in S can be compensated for by a decrease in η . For $\eta_{10} \approx 6$ and $S - 1 \ll 1$, a good approximation (for fixed D) is $\Delta\eta_{10} \approx 6(S - 1)$ (Kneller & Steigman 2003). In Figure 8 are shown the ${}^4\text{He} - \text{D}$ (Y_{P} versus D/H) relations for three values of the expansion rate parameterized by N_ν . To first order, the combination of η and S that recovers the SBBN deuterium abundance will leave the ${}^3\text{He}$ abundance prediction unchanged as well, preserving its good agreement with the observational data. However, the consequences for ${}^7\text{Li}$ are not so favorable. The BBN abundance of ${}^7\text{Li}$ increases with decreasing S but decreases with a smaller η ; the two effects nearly cancel leaving essentially the same discrepancy as for SBBN. For ${}^7\text{Li}$, a nonstandard expansion rate cannot relieve the tension between the BBN prediction and the observational data.

Setting aside ${}^7\text{Li}$, it is of interest to consider the simultaneous constraints from BBN on the baryon density parameter and the expansion rate factor from the abundances of D and ${}^4\text{He}$; it has already been noted that for this nonstandard case, D and ${}^3\text{He}$ will remain consistent. In Figure 9 are shown the 1σ , 2σ , and 3σ contours in the $\Delta N_\nu - \eta$ plane derived from BBN and the D and ${}^4\text{He}$ relic abundances. As expected from the discussion above, the best fit value of η (the cross in Figure 9) has shifted downward to $\eta_{10} = 5.7$ ($\omega_{\text{B}} = 0.021$). While the best fit is for $\Delta N_\nu = -0.7$ ($S = 0.94$), it should be noted that the standard case of $N_\nu = 3$ is entirely compatible with the data at the $\sim 2\sigma$ level.

8. Nonstandard CBR: $S \neq 1$, $N_\nu \neq 3$

The CBR temperature fluctuation anisotropy spectrum is sensitive to the early-Universe radiation density (ρ_{R}) as well as to the overall expansion rate. The early Universe is radiation dominated so that $\rho \approx \rho_{\text{R}} \propto 1 + 0.135\Delta N_\nu$ (see Eq. 2.6 and recall that $\rho \propto H^2$). The late Universe is matter dominated (MD) ($\omega_{\text{M}} \equiv \Omega_{\text{M}}h^2$) and the crossover from RD to MD, important for the growth of fluctuations and for the age/size of the Universe at

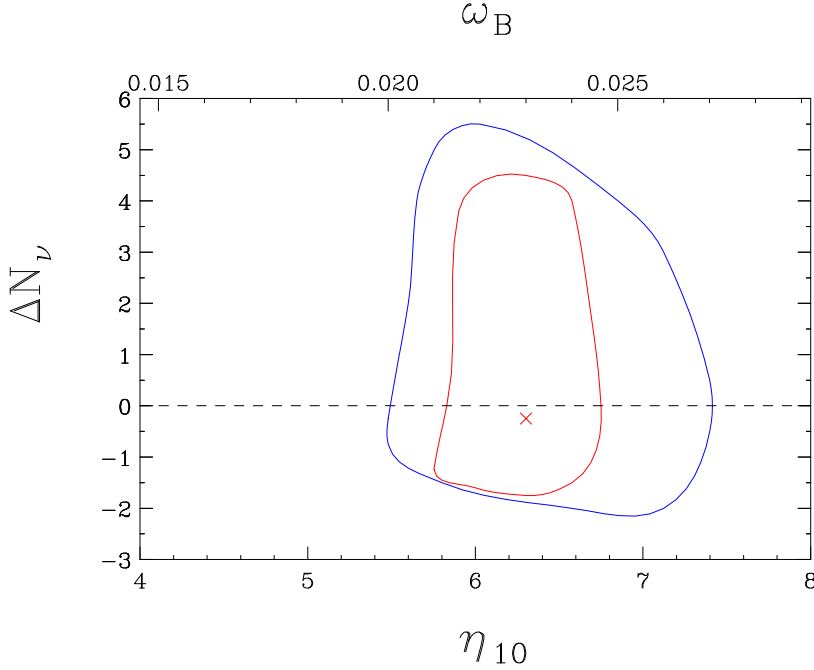


FIGURE 10. The 1σ and 2σ contours in the $\eta - \Delta N_\nu$ plane from the CBR (*WMAP*) data. The best fit point ($\eta_{10} = 6.3$, $\Delta N_\nu = -0.25$) is indicated by the cross.

recombination, occurs for a redshift

$$z_{eq} = 2.4 \times 10^4 \omega_M (1 + 0.135 \Delta N_\nu)^{-1}. \quad (8.1)$$

If the matter content is kept fixed while the radiation content is increased, corresponding to a faster than standard expansion rate, matter-radiation equality is delayed, modifying the growth of fluctuations prior to recombination and, also, the Universe is younger at recombination and has a smaller sound horizon, shifting the angular location of the acoustic peaks. The degeneracy between the radiation density (ΔN_ν or S) and ω_M is broken by the requirement that $\Omega_M + \Omega_\Lambda = 1$ and the HST Key Project determination of the Hubble parameter (see Barger *et al.* (2003a) for details and further references). In Figure 10 are shown the 1σ and 2σ contours in the $\Delta N_\nu - \eta$ plane from the CBR (*WMAP*) data; note the very different ΔN_ν scales and ranges in Figures 9 and 10. As is the case for BBN (see §7), the CBR favors a slightly slower than standard expansion. However, while the “best” fit value for the expansion rate factor is at $S < 1$ ($\Delta N_\nu < 0$), the CBR likelihood distribution of ΔN_ν values is very shallow and the *WMAP* data are fully consistent with $S = 1$ ($\Delta N_\nu = 0$).

Comparing Figures 9 and 10, it is clear that for this variant of the standard cosmology there is excellent overlap between the $\eta - \Delta N_\nu$ confidence contours from BBN and those from the CBR (see Barger *et al.* 2003a). This variant of SBBN ($S \neq 1$) is consistent with the CBR. In Figure 11 (from Barger *et al.* 2003a) are shown the confidence contours in the $\eta - \Delta N_\nu$ plane for a joint BBN – CBR fit. Again, while the best fit value for ΔN_ν is negative (driven largely by the adopted value for Y_P), $\Delta N_\nu = 0$ ($S = 1$) is quite acceptable.

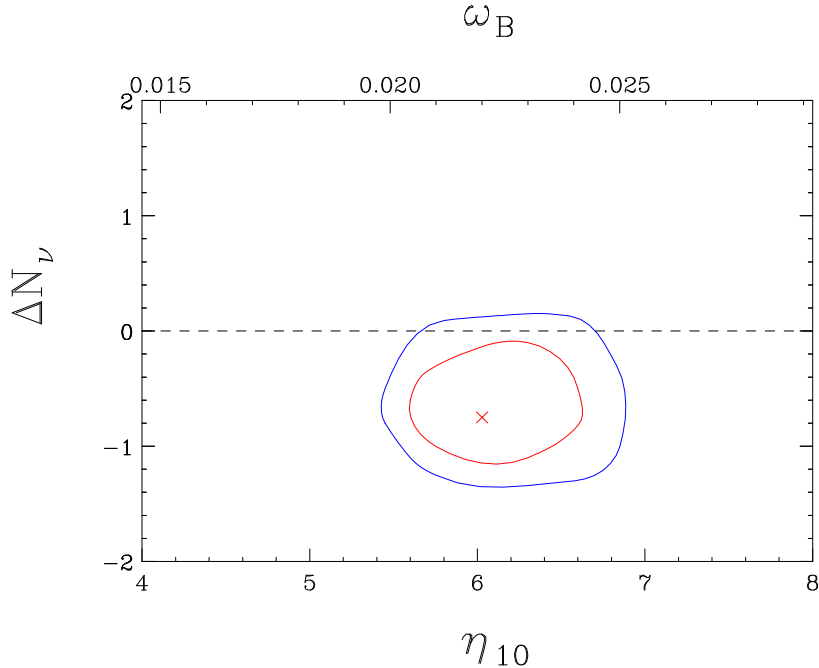


FIGURE 11. As for Figure 10, but for the *joint* BBN – CBR fit. The best fit point ($\eta_{10} = 6.0$, $\Delta N_\nu = -0.75$) is indicated by the cross.

9. Summary And Conclusions

As cosmology deals with an abundance of precision data, redundancy will be the key to distinguishing systematic errors from evidence for new physics. BBN and the CBR provide complementary probes of the Universe at two epochs widely separated from each other and from the present. For the standard model assumptions ($N_\nu = 3$, $S = 1$) the SBBN-inferred baryon density is in excellent agreement with that derived from the CBR (with or without the extra constraints imposed by large scale structure considerations and/or the Lyman alpha forest). For this baryon density ($\eta_{10} \approx 6.1$, $\omega_B \approx 0.022$), the SBBN-predicted abundances of D and ${}^3\text{He}$ are in excellent agreement with the observational data. For ${}^4\text{He}$ the predicted relic mass fraction is $\sim 2\sigma$ higher than the primordial abundance inferred from current data, hinting at either new physics or the presence of unidentified systematic errors. For ${}^7\text{Li}$ too, the SBBN-predicted abundance is high compared to that derived from very metal-poor stars in the Galaxy. While the tension with ${}^4\text{He}$ can be relieved by invoking new physics in the form of a nonstandard (slower than expected) early-Universe expansion rate, this choice will not reconcile the BBN-predicted and observed abundances of ${}^7\text{Li}$. When *both* the baryon density and the expansion rate factor are allowed to be free parameters, BBN (D, ${}^3\text{He}$, and ${}^4\text{He}$) and the CBR (WMAP) agree at 95% confidence for $5.5 \leq \eta_{10} \leq 6.8$ and $1.65 \leq N_\nu \leq 3.03$.

The engine powering the transformation of the study of cosmology from its youth to its current maturity has been the wealth of observational data accumulated in recent years. In this data-rich, precision era BBN, one of the pillars of modern cosmology, continues to play a key role. The spectacular agreement between the estimates of the baryon density derived from processes at widely separated epochs has confirmed the general

assumptions of the standard models of cosmology and of particle physics. The tension with ^4He (and with ^7Li) provides a challenge, along with opportunities, to cosmology, to astrophysics, and to particle physics. Whether the resolution of these challenges is observational, theoretical or, a combination of both, the future is bright.

I am grateful to all my collaborators and I am happy to thank them for their various contributions to the material reviewed here. Many of the quantitative results (and figures) presented here are from recent collaborations or discussions with V. Barger, J. P. Kneller, H.-S. Lee, J. Linsky, D. Marfatia, K. A. Olive, R. J. Scherrer, V. V. Smith, and T. P. Walker. My research is supported at OSU by the DOE through grant DE-FG02-91ER40690. This manuscript was prepared while I was visiting the Instituto Astrônomico e Geofísico of the Universidade de São Paulo, and I thank them for their hospitality.

REFERENCES

- ALLENDE-PRieto, C., LAMBERT D. L. & ASPLUND M. 2001 *Astrophys. J. Lett.* **556**, L63.
 BANIA, T., ROOD, R. T. & BALSER, D. 2002 *Nature* **415**, 54.
 BARGER, V., KNELLER, J. P., LEE, H.-S., MARFATIA, D., & STEIGMAN, G. 2003a *Phys. Lett. B* **566**, 8.
 BARGER, V., KNELLER, J. P., MARFATIA, D., LANGACKER, P. & STEIGMAN, G. 2003b *Phys. Lett. B* **569**, 123.
 BENNETT, C. L. *et al.* 2003 *Astrophys. J. Suppl.* **148**, 1.
 BINETRUY, P., DEFAYYET, C., ELLWANGER, U. & LANGLOIS, D. 2000 *Phys. Lett. B* **477**, 285.
 BURLES, S., NOLLETT, K. M. & TURNER, M. S. 2001 *Phys. Rev. D* **63**, 063512.
 CLINE, J. M., GROJEAN, C. & SERVANT, G. 2000 *Phys. Rev. Lett.* **83**, 4245.
 DEARBORN, D. S. P., STEIGMAN, G. & SCHRAMM, D. N. 1986 *Astrophys. J.* **203**, 35.
 DEARBORN, D. S. P., STEIGMAN, G. & TOSI, M. 1996 *Astrophys. J.* **465**, 887.
 GEISS, J. & GLOECKLER, G. 1998 *Space Sci. Rev.* **84**, 239.
 GRUENWALD, R., STEIGMAN, G. & VIEGAS, S. M. 2002 *Astrophys. J.* **567**, 931.
 IBEN, I., JR. 1967 *Astrophys. J.* **147**, 624.
 IZOTOV, Y. I., THUAN T. X. & LIPOVETSKY V. A. 1997 *Astrophys. J. Suppl.* **108**, 1.
 IZOTOV, Y. I. & THUAN, T. X. 1998 *Astrophys. J.* **500**, 188.
 KIRKMAN, D., TYTLER, D., SUZUKI, N., O'MEARA, J. M. & LUBIN, D. 2003 *Astrophys. J. Suppl.* **submitted**, (astro-ph/0302006).
 KNELLER, J. P. & STEIGMAN, G. 2003 BBN For Pedestrians., *In Preparation*.
 O'MEARA, J. M., TYTLER, D., KIRKMAN, D., SUZUKI, N., PROCHASKA, J. X., LUBIN, D. & WOLFE, A. M. 2001 *Astrophys. J.* **552**, 718.
 OLIVE, K. A. & STEIGMAN, G. 1995 *Astrophys. J. Suppl.* **97**, 49.
 OLIVE, K. A., SKILLMAN, E. & STEIGMAN, G. 1997 *Astrophys. J.* **483**, 788.
 OLIVE, K. A. & SKILLMAN, E. 2001 *New Astron.* **6**, 119.
 OLIVE, K. A., STEIGMAN, G. & WALKER, T. P. 2000 *Phys. Rep.* **333**, 389.
 PEIMBERT, A., PEIMBERT, M. & LURIDIANA, V. 2002 *Astrophys. J.* **565**, 668.
 PINSONNEAULT, M. H., STEIGMAN, G., WALKER, T. P. & NARAYANAN, V. K. 2002 *Astrophys. J.* **574**, 398.
 RANDALL, L. & SUNDRUM, R. 1999a *Phys. Rev. Lett.* **83**, 3370.
 RANDALL, L. & SUNDRUM, R. 1999b *Phys. Rev. Lett.* **83**, 4690.
 RYAN, S. G., BEERS, T. C., OLIVE, K. A., FIELDS, B. D. & NORRIS, J. E. 2000 *Astrophys. J. Lett.* **530**, L57.
 SAUER, D. & JEDAMZIK, K. 2002 *Astron. & Astrophys.* **381**, 361.
 SPERGEL, D. N. *et al.* 2003 *Astrophys. J. Suppl.* **148**, 175.
 STEIGMAN, G., SCHRAMM, D. N. & GUNN, J. E. 1977 *Phys. Lett. B* **66**, 202.
 STEIGMAN, G., VIEGAS, S. M. & GRUENWALD, R. 1997 *Astrophys. J.* **490**, 187.
 VASSILIADIS, E. & WOOD, P. R. 1993 *Astrophys. J.* **413**, 641.
 VIEGAS, S. M., GRUENWALD, R. & STEIGMAN, G. 2000 *Astrophys. J.* **531**, 813.